# mTORC1 upregulation via ERK-dependent gene expression change confers intrinsic resistance to MEK inhibitors in oncogenic KRas-mutant cancer cells.

AUTHOR(S):

Komatsu, Naoki; Fujita, Yoshihisa; Matsuda, Michiyuki; Aoki, Kazuhiro

CITATION:

Komatsu, Naoki ...[et al]. mTORC1 upregulation via ERK-dependent gene expression change confers intrinsic resistance to MEK inhibitors in oncogenic KRas-mutant cancer cells.. Oncogene 2015, 34(45): 5607-5616

ISSUE DATE:

2015-11-05

URL:

http://hdl.handle.net/2433/207613

**Title**

mTORC1 upregulation via ERK-dependent gene expression change confers intrinsic resistance to MEK inhibitors in oncogenic KRas-mutant cancer cells.

**Authors**

Naoki Komatsu[1], Yoshihisa Fujita[2], Michiyuki Matsuda[1,2], and Kazuhiro Aoki[3]

**Affiliations**

1. Laboratory of Bioimaging and Cell Signaling, Graduate School of Biostudies, Kyoto University, Japan

2. Department of Pathology and Biology of Diseases, Graduate School of Medicine, Kyoto University, Japan

3. Imaging Platform for Spatio-Temporal Information, Graduate School of Medicine, Kyoto University, Japan

**To whom correspondence should be addressed**

Kazuhiro Aoki, Imaging Platform for Spatio-Temporal Information, Graduate School of Medicine, Kyoto University, Sakyo-ku, Kyoto 606-8501, Japan; Tel.: 81-75-753-9450; Fax: 81-75-753-4698; E-mail: k-aoki@lif.kyoto-u.ac.jp

**Running title (less than 50 letters and spaces):**

Transcriptional control of mTORC1 activity by ERK

## Abstract

Cancer cells harboring oncogenic *BRaf* mutants, but not oncogenic *KRas* mutants, are sensitive to MEK inhibitors (MEKi). The mechanism underlying the intrinsic resistance to MEKi in KRas-mutant cells is under intensive investigation. Here, we pursued this mechanism by live imaging of ERK and mTORC1 activities in oncogenic KRas or BRaf mutant cancer cells. We established eight cancer cell lines expressing FRET biosensors for ERK activity and S6K activity, which was used as a surrogate marker for mTORC1 activity. Under increasing concentrations of MEKi, ERK activity correlated linearly with the cell growth rate in BRaf-mutant cancer cells, but not KRas-mutant cancer cells. Administration of PI3K inhibitors resulted in a linear correlation between ERK activity and cell growth rate in KRas-mutant cancer cells. Intriguingly, mTORC1 activity was correlated linearly with the cell growth rate in both BRaf-mutant cancer cells and KRas-mutant cancer cells. These observations suggested that mTORC1 activity played a pivotal role in cell growth and that the mTORC1 activity was maintained primarily by the ERK pathway in BRaf-mutant cancer cells and by both the ERK and PI3K pathways in KRas-mutant cancer cells. FRET imaging revealed that MEKi inhibited mTORC1 activity with slow kinetics, implying transcriptional control of mTORC1 activity by ERK. In agreement with this observation, MEKi induced the expression of negative regulators of mTORC1, including TSC1, TSC2, and Deptor, which occurred more significantly in BRaf-mutant cells than in KRas-mutant cells. These findings suggested that the suppression of mTORC1 activity and induction of negative regulators of mTORC1 in cancer cells treated for at least one day could be used as surrogate markers for the MEKi sensitivity of cancer cells.

**Keywords:**

FRET imaging/MEK inhibitor/Intrinsic resistance

## Introduction

The Ras-Raf-MEK-ERK signalling pathway plays a central role in cell proliferation, differentiation and survival.[1] Gain-of-function mutations in the Ras-Raf-MEK-ERK pathway have frequently been observed in various cancers, including melanoma, pancreatic cancer, lung cancer, colorectal cancer, and breast cancer.[2] These mutations induce hyper-activation of the pathway, culminating in the induction of cancers.

The growth of many cancer cells depends on a specific driving oncogene, a phenomenon known as “oncogene addiction.”[3, 4] This idea has been well-established in *BCR-ABL*-induced chronic myelogenous leukemias and *EGFR* mutant non-small lung cancer.[5] Therefore, targeting molecules in the Ras-Raf-MEK-ERK pathway could be a promising therapeutic strategy. MEK inhibitors (MEKi) have been tested in early-phase clinical trials as BRaf inhibitors (BRafi).[6] Cancer cells harboring *BRaf* mutation undergo G1 cell cycle arrest and apoptosis by BRafi and MEKi treatment,[7] clearly indicating that *BRaf*-mutant cancer cells are “addicted” to the ERK pathway. Several cancer cell lines harboring active *KRas* mutations also exhibit oncogene addiction, which is manifested by induction of cell cycle arrest and apoptosis by silencing of *KRas* expression.[8] Unlike BRaf-mutant cancer cells, Ras-mutant cancer cells are less sensitive to MEKi.[7] In Ras-mutant cells, MEKi demonstrates a cytostatic effect rather than cytotoxic activity.[6]

Resistance to targeted drugs has emerged as a critical issue in the clinical outcome of anticancer therapy. There exist two mechanisms by which cancer cells demonstrate resistance to targeted drugs: an intrinsic and an acquired mechanism.[9] Intrinsic resistance is caused by genetic and/or epigenetic alterations existing before treatment. On the other hand, acquired resistance is induced by drug treatment over a long period, and it can be due to gene mutation, overexpression or silencing acquired after treatment. The low sensitivity to MEKi in the Ras-mutant cancer cells is an example of intrinsic resistance. One of the possible mechanisms by which oncogenic Ras mutants, but not oncogenic BRaf mutants, render cancer cells resistant to MEKi is the presence of feedback loops and cross-talk between Ras and other pathways, such as the EGFR pathway and the PI3K-Akt-mTOR pathway.[6, 10] For example, it has been reported that inhibition of ERK by MEKi releases negative feedback from ERK to CRaf,

thereby increasing phosphorylated MEK and decreasing drug efficacy.[11-13] Intriguingly, the BRaf V600E mutant disrupts the negative feedback from ERK to CRaf.[12, 14] In addition, cross-talk between the Ras-ERK and PI3K-Akt-mTOR pathways is involved in the intrinsic resistance. Indeed, MEKi treatment causes Akt phosphorylation, which determines the susceptibility of cancer cells to MEK inhibition.[10, 15]

To overcome MEKi resistance in KRas-mutant cancer cells, the logical approach would be a combination of strategies using MEKi to induce cytotoxicity. One of the promising combinations is MEKi plus PI3K/mTOR or Akt inhibitors,[16, 17] and these clinical trials are ongoing,[6] although toxicity of both inhibitors limits the maximally tolerated doses that can be used in combination.[18, 19] However, it is unclear to what extent *KRas*-mutant cancer cells are addicted to either the Ras-ERK pathway or the PI3K-Akt-mTOR pathway, or what roles feedback and cross-talk play in the process of intrinsic resistance in these cells.

Here, we have addressed this issue by monitoring the effects of MEKi on ERK and mTORC1 activities and cell growth with live-cell imaging in BRaf- or KRas-mutant cancer cells. We found that MEKi-induced suppression of ERK activity was linearly correlated with the reduction of mTORC1 activity and cell growth rate in BRaf-mutant cancer cells, but not in KRas-mutant cells. The MEKi-induced suppression of mTORC1 activity was markedly slower than the ERK suppression. In agreement with this finding, we found that several genes involved in the regulation of mTORC1 activity were transcriptionally regulated.

## Results

*Linear correlation between ERK activity and cell growth rate upon MEKi treatment in BRaf-mutant cells, but not in KRas-mutant cells.*

To address the mechanisms of MEKi resistance in cancer cells, we designed a live-cell imaging platform by which the molecular activity and cell growth rate in cancer cells could be simultaneously monitored in the presence of various inhibitors (Figure 1a and 1b). For the analysis, we chose 6 cell lines that harbor oncogenic mutations of *BRaf* or *KRas*, and 2 cell lines that are not known to have any oncogenic mutations of *BRaf* and *KRas* (Supplementary Table 1). The cell lines were stably expressed with a FRET biosensor for ERK activity,

EKAREV-nls, or for S6K activity, Eevee-S6K.[20] After the addition of inhibitor, cells were monitored for the kinase activity and cell number every day (Figure 1b).

First, we examined the dose effect of AZD6244, a potent MEKi, on the ERK activity and growth rate of HT-29 cells bearing the V600E *BRaf* mutation and HCT116 cells bearing the G13D *KRas*. HT-29 cells exhibited almost identical IC50 values for both ERK activity ($0.030 \pm 0.0045$ μM) and cell growth rate ($0.064 \pm 0.024$ μM) (Figure 1c), resulting in a linear correlation between ERK activity and cell growth rate (Figure 1d). On the other hand, in HCT116 cells the IC50 of $1.2 \pm 0.32$ μM for the cell growth rate was approximately 50-fold higher than the IC50 of $0.023 \pm 0.0034$ μM for ERK activity, resulting in a non-linear correlation between ERK activity and growth rate (Figure 1e and 1f). The resistance of HCT116 to MEKi was as reported by Friday et al.[12] Importantly, a linear correlation between ERK activity and cell growth rate was observed in all three BRaf-mutant cell lines, but not in the KRas-mutant cell lines (Figure 1g). ERK activity in KRas-mutant cells was slightly restored one day after MEKi treatment (Supplementary Figure S1). In cell lines without known mutation of BRaf or KRas, no clear tendency could be identified (Figure 1g). Taken together, these results showed that the cell growth rate was entirely dependent on ERK activity in BRaf-mutant cells, but not in KRas-mutant cells. There are several possible explanations for the inhibition of the cell growth of KRas-mutant cells by a high dose of MEKi—e.g., very low ERK activity may have been sufficient to maintain the cell growth of KRas-mutant cells, or alternatively, the ERK activity may have been dispensable, but other kinases that are indispensable for cell growth could have been inhibited at high concentrations of MEKi. In any event, the use of high-dose MEKi as a therapeutic is clinically impractical if we take the adverse effects of MEKi into account.[21]

*Dependence of cell growth on the PI3K-Akt-mTOR pathway*

If ERK is dispensable for the cell growth of KRas-mutant cells, does the PI3K-Akt-mTOR pathway support the proliferation of these cells? To answer this question, we examined the effect of inhibitors against EGFR, BRaf, MEK, RSK, PI3K, and mTOR on cell growth (Figure 2a). To compare the sensitivity among 8 cell lines, we used a relative resistance index,

which we calculated by dividing the IC50 value for a given inhibitor in each cell line by the lowest IC50 value for that inhibitor among all 8 cell lines (Figure 2b). The sensitivity of the cell lines was analysed by clustering (Figure 2c). As expected, the cell lines were clustered into two groups, the BRaf-mutant cell lines and the others. The BRaf-mutant cell lines were more sensitive to BRafi/MEKi than the KRas-mutant cell lines or *KRas* and *BRaf* WT cell lines (Figure 2c). On the other hand, the BRaf-mutant cell lines were more resistant to the PI3K inhibitor and mTOR inhibitor than the KRas-mutant cell lines and *KRas* and *BRaf* WT cell lines, suggesting that the MEKi-resistant cell lines were more dependent on PI3K-Akt-mTOR signalling for cell growth than were the BRaf-mutant cell lines. Therefore, if the PI3K-Akt-mTOR pathway was abrogated, would the KRas-mutant cell lines exhibit linear correlation of ERK activity with cell growth rate, as was the case in BRaf-mutant cell lines? To answer this question, we examined the correlation between the ERK activity and cell growth rate of BRaf-mutant HT-29 cells and KRas-mutant HCT116 cells in the presence of increasing concentrations of MEKi and PI3K inhibitor (PI3Ki)(Figure 2d-g). HT-29 cells demonstrated the linear correlation between ERK activity and cell proliferation rate regardless of the treatment of PI-103, a PI3Ki (Figure 2e). On the contrary, PI-103 treatment sensitized HCT116 cells to MEKi; the cell growth rate was linearly correlated with ERK activity in the presence of 1 μM PI-103 (Figure 2g, light green dots). We further analyzed ERK activity distribution at the single cell level in HT-29 cells and HCT116 cells (Supplementary Figure S2). ERK activity followed normal bell-shape distribution, and gradually decreased by MEK inhibition with the bell-shape distribution keeping in both HT-29 cells and HCT116 cells. These results strongly suggested that the signals from the Raf-MEK-ERK pathway and PI3K-Akt-mTOR pathway converged on a molecule that controls the cell growth of HCT116 cells, and probably also the other KRas-mutant or BRaf-mutant cancer cells.

*Linear correlation between S6K activity and cell growth rate in both BRaf- and KRas-mutant cells.*

We assumed that mTORC1 was a key cell growth controller functioning downstream of ERK and PI3K. To examine the correlation of mTORC1 activity with the cell growth rate, we

established cell lines expressing the S6K FRET biosensor, Eevee-S6K, which was used as a surrogate marker for mTORC1 activity. The S6K activity was decreased in a manner dependent on cell density in both HT-29 and HCT116 cells (Figure 3a-c). In HT-29 cells, MEKi slowly suppressed S6K activity in a dose-dependent manner from one day after treatment (Figure 3a). In contrast, PI-103 treatment decreased S6K activity within 20 min, but the effect was cancelled in 1-2 days (Figure 3b). These observations suggested that ERK regulates mTORC1 in a transcription-dependent manner, and that the same mechanism may operate to cancel the PI3Ki-induced decrease of S6K activity in HT-29 cells. HCT116 cells showed higher basal S6K activity than HT-29 cells, and also slow inhibition of S6K activity by MEKi from one day after treatment as observed in HT-29 cells (Figure 3c). The effect of PI3Ki on S6K was rapid and sustained in HCT116 cells (Figure 3d). Interestingly, in clear contrast to ERK activity (Figure 2e and 2g), cell growth rate was linearly correlated with S6K activity in both HT-29 cells and HCT116 cells in the combined application of MEKi and PI3Ki (Figure 3e and 3f, Supplementary Figure S3). S6K activity at the single cell level in HCT116 cells showed broader and more biased distribution than that in HT-29 cells (Supplementary Figure S4). MEK inhibition suppressed S6K activity in the approximately half of HCT116 cells (Supplementary Figure S4b, upper left), and additional PI3K inhibition lead to the reduction of S6K activity in the remaining half of cells. These results implied that mTORC1/S6K activity regulated the cell growth rate, and that the MEKi resistance of *KRas*-mutant cell lines was due to the mTORC1/S6K activity remaining in the presence of MEKi. To confirm this observation, we quantified the phosphorylation of Rictor Thr1135, an S6K substrate. The basal phosphorylation level was lower in HT-29 cells than HCT116 cells (Figure 3g and 3h). . MEKi decreased pRictor/Rictor, but the remaining pRictor/Rictor value was markedly larger in HCT116 cells than in HT-29 cells (Figure 3h, arrows), which was consistent with the imaging data (Figure 3a and 3c, arrows). We also examined these results in other cell lines and found that MEKi treatment could not induce a sufficient reduction of Rictor Thr1135 phosphorylation in MEKi-resistant cells (Supplementary Figure S5). Taken together, the mTORC1/S6K activity correlated with cell growth, and the reduction of mTORC1/S6K activity induced by MEKi represented the sensitivity to the MEKi.

*Requirement of rapamycin-insensitive mTORC1 activity for cell growth in MEKi-resistant and MEKi-sensitive cells.*

To identify which molecules regulated cell growth most directly, we systematically perturbed components of the PI3K/mTOR pathway by chemical inhibitors, gene depletion by siRNAs or CRISPR/Cas9 system, and dominant negative mutants, and examined the effects on S6K activity and cell growth. PI-103 and Torin1, an mTORC1/2 inhibitor, reduced the S6K activity and growth rate in a dose-dependent manner in both HT-29 cells and HCT116 cells (Figure 4a, 4b, 4d and 4e). Rapamycin did not suppress cell growth even though rapamycin treatment robustly decreased S6K activity (Figure 4c and 4f). The depletion of Raptor, a critical component of mTORC1, by RNAi or CRISPR/Cas9 inhibited both S6K activity and the cell growth rate (Figure 4g-4l). Therefore, a rapamycin-insensitive target of mTORC1, but not S6K, played a critical role in cell growth.[22] A candidate molecule would be 4E-BP1.[23] To examine whether this molecule was in fact the target of mTORC1, we employed a tetracycline-inducible expression of dominant negative mutant of 4E-BP1, 4E-BP1 4A, for the inhibition of 4E-BP1 function. The expression of the dominant negative mutant of 4E-BP1 clearly suppressed the proliferation of A375, HT-29, and HCT116 cells (Figure 4m). These results indicated that mTORC1-activated 4E-BP1 was required for cell growth in both MEKi-sensitive and -resistant cells. Therefore, the different sensitivity to MEKi between BRaf-mutant and KRas-mutant cells was attributed to the mechanisms by which ERK activity regulated mTORC1 activity.

*MEKi treatment-induced global change in gene expression in mTORC1 pathway components.*

How does the Raf-MEK-ERK pathway regulate mTORC1? Although the post-translational mechanisms could be considered such as negative feedbacks and cross-talk between ERK and mTORC1 pathway (see Discussion), the slow inhibition of mTORC1/S6K activity by MEKi (Figure 3a and 3c) prompted us to examine the transcriptional/translational regulation of mTORC1 by ERK. To test this hypothesis, the gene expression profile was compared between cells cultured in the presence and absence of a MEKi, PD0325901 (Figure 5a). We

identified 8428 and 7786 genes in HT-29 cells and HCT116 cells, respectively, as differentially expressed genes (DEGs) (Figure 5b and 5c). Among them, we focused on genes that are related to mTORC1 signalling. Upon MEKi treatment, 3 out of 9 positive regulators for the mTORC1 signalling pathway were down-regulated, i.e., *Akt1*, *Rheb*, and *Raptor* whereas 4 out of 5 negative regulators were up-regulated, i.e., *TSC1*, *TSC2*, *DEPTOR*, and *REDD1* (Figure 5d). Of note, these down- and up-regulated mTORC1-related genes were more evident in HT-29 cells than in HCT116 cells. To check whether the change in gene expression pattern was also observed in other cell lines, the expression levels of these genes were quantified by qPCR. We found that the up-regulation of *TSC2* and *DEPTOR* genes was more significant in BRaf-mutant cells than in KRas-mutant cells (Figure 5e). We speculated that up-regulation of *TSC2* and *DEPTOR* would be a mechanism for mTORC1 inactivation by MEKi. However, depletion of TSC2 or DEPTOR by RNAi did not affect S6K activity or cell growth in the presence of MEKi in BRaf-mutant cells (Supplementary Figure S6 and S7). The knockdown of either *TSC*2 or *DEPTOR* might be insufficient to rescue MEKi-induced mTORC1 inactivation. Taken together, these results lead us to suggest that ERK inactivation upon MEKi treatment induces the global change in gene expressions related to mTORC1 signalling, and the alteration of these genes cooperatively results in the mTORC1 inactivation and cell growth inhibition.

## Discussion

Based on the results of the present experiments, we propose that the following mechanism underlies the difference of MEKi sensitivity between BRaf- and KRas-mutant cancer cells (Figure 6). In both BRaf- and KRas-mutant cancer cells, mTORC1 activity is a bottleneck for cell proliferation and survival. In BRaf-mutant cancer cells, mTORC1 activity is regulated primarily by ERK activity, which is inferred from the linear correlation of ERK activity with mTORC1 activity in the presence of various concentrations of MEKi (Figure 6a). By contrast, KRas-mutant cancer cells employ both ERK and PI3K-Akt pathways to maintain mTORC1 activity, and therefore MEKi monotherapy cannot significantly reduce the mTORC1 activity and cell growth (Figure 6b). This could be due to KRas activation of the PI3K-Akt-mTORC1

pathway through the direct binding of KRas to p110 catalytic subunits of PI3K.[26] In the cell lines used in the present research, neither the presence of *PI3K* mutation nor the presence of *PTEN* mutation was correlated with the sensitivity to PI3Ki and mTORC1/2 inhibitor (Figure 2c and Supplementary Table S1). Intriguingly, the drug sensitivities of *Ras* WT and *BRaf* WT cancer cells were found to be equivalent to those of KRas-mutant cancer cells by clustering (Figure 2c). The data implicate that oncogenic BRaf mutation reduces PI3K-Akt dependency and subsequently increases ERK dependency on mTORC1 activity.

Our data suggest that mTORC1 activity is transcriptionally regulated by ERK. The Ras-ERK pathway activates the PI3K-Akt-mTORC1 pathway by multiple mechanisms.[27] It has been shown that ERK and RSK, a downstream molecule of ERK, phosphorylate and inactivate TSC2, a component of Rheb GAP, leading to the activation of Rheb and mTORC1.[24] A similar mechanism has been proposed for Raptor; ERK and RSK phosphorylate Raptor and promote tumorigenesis through 4E-BP phosphorylation.[25] However, the ERK and/or RSK-mediated phosphorylation of the regulators of mTORC1 does not seem to play a major role in maintaining the mTORC1 activity of the cell lines used in the present study, because we found that MEKi decreased mTORC1 activity with slow kinetics requiring nearly one day of treatment for full suppression (Figure 3a and 3c). It should be noted that the observed slow kinetics was not due to the kinetics of the FRET biosensor, which could capture the fast mTORC1 inactivation by PI3Ki or rapamycin (Figure 3b and 3d).[20] In support of our proposal, we observed increases in the negative regulators of mTORC1, including *TSC1*, *TSC2*, *Deptor*, and *REDD1*, upon MEKi treatment (Figure 5d). Related to this issue, we failed to observe any significant effect of knockdown of *TSC2* or *Deptor* on the sensitivity of BRaf mutant cells to MEKi (Supplementary Figure S6 and S7). However, this observation does not necessarily negate the role of the negative regulators of mTORC1 on the ERK-mediated mTORC1 activation. Even though the effect of ERK activity on the expression of each gene is modest, it is possible that global suppression of the genes of negative regulators may have a profound effect. Thus, we suggest that the different sensitivity to MEKi between BRaf- and KRas-mutant cells is caused by the level of dependency on the ERK-mediated mTORC1 activation.

Other possible mechanisms that could have contributed to the difference of MEKi sensitivity between BRaf- and Ras-mutant cells are: (1) the negative feedback from ERK to Raf, which is abrogated in BRaf-mutant cells,[12-14] and (2) the negative feedback from ERK to EGFR[28, 29]. As for the negative feedback from ERK to Raf, we observed a slight restoration of ERK activity in KRas-mutant cells one day after MEKi treatment (Supplementary Figure S1). However, the increase in IC50 values of ERK activity was ~ 2 fold, which was unlikely to explain the ~ 50-fold difference in the IC50 values for cell growth (Figure 1e). These data were essentially consistent with the previous study.[12] As for the negative feedback from ERK to EGFR, unlike in the previous reports[28, 29], we could not reproduce MEKi-induced activation of Akt in our experimental condition, namely in the presence of 10% serum condition (Supplementary Figure S8). Consistent with this result, no decrease of cell growth rate and S6K activity was observed by the additional treatment of an EGFR inhibitor, Gefitinib (Supplementary Figure S9). We confirmed that the concentration of Gefitinib used in the analyses was sufficient to suppress EGFR activation (Supplementary Figure S10). These results supported our claim that ERK regulates mTORC1 activity through transcriptional mechanisms, though we have not yet obtained direct experimental evidences.

An important message from this study is that the sensitivity of mTORC1 to MEKi could be used as a promising surrogate marker of cancer cells for MEKi sensitivity. In this study, as an indicator of mTORC1 activity we employed S6K-mediated phosphorylation of Rictor at Thr1135, which was detected either by the FRET biosensor Eevee-S6K or anti-phospho-Rictor (Thr1135) antibody. In line with this view, phospho-S6 (Ser240/S244) and phospho-S6 (Ser235/S236) have been used as markers of resistance to MEKi in melanoma cells.[30] Importantly, the suppression of mTORC1 activity was observed only at one day after MEKi treatment, when the mRNAs of TSC2 and DEPTOR were increased. Therefore, by measuring the S6K activity or expression levels of *TSC2* and *DEPTOR* in patient samples pretreated with MEKi for one day, we may be able to predict the sensitivity of cancer cells to MEKi.

## Materials and Methods

*Cell culture.*

The cell lines HCT116, A549, NCI-H460 and MCF10A were obtained from ATCC (American Type Culture Collection). The cell lines HT-29, A375 and LIM1215 were obtained from ECACC (European Collection of Cell Cultures). HEK-293T cells were purchased from Clontech (Mountain View, CA). Colo205 cells were the kind gift of Dr. Won Do Heo (KAIST, Korea). A549, A375 and HEK-293T cells were maintained in DMEM (Sigma-Aldrich, St. Louis, MO). HCT116 and HT-29 cells were grown in McCoy's 5A medium (Sigma-Aldrich). NCI-H460 and Colo205 cells were cultured in RPMI1640 (Sigma-Aldrich). LIM1215 cells were maintained in DMEM/F12 (Sigma-Aldrich). The growth media described above were supplemented with 10% fetal bovine serum (FBS) and penicillin/streptomycin. MCF10A cells were grown in mammary epithelial basal medium (Cell Applications, CA) supplemented with the growth supplements (Cell Applications) and 100 ng/ml cholera toxin (BioAcademia, Tokyo, Japan). All cells were incubated in a humidified atmosphere of 5% $CO_2$ at 37°C.

*Plasmids and establishment of stable cell lines.*

FRET biosensors for ERK activity with a nuclear localization signal, EKAREV-nls, and for S6K activity with a nuclear exporting signal, Eevee-S6K, were described previously.[20] cDNAs of EKAREV-nls or Eevee-S6K were subcloned into pPBbrs vector, a PiggyBac transposon vector[31] with IRES-*bsr* (blasticidin S resistant gene), pT2Apuro vector, a Tol2 transposon vector[32] with IRES-*pac* (puromycin resistant gene), or pCSIIbsr-EF, a lenti-virus vector[33] with IRES-*bsr*. mCherry tagged with tandem repeats of NLS, mCherry-NLSx2, was introduced into the pCX4neo retrovirus vector.[34] pCW57.1-4E-BP1 4xAla and lentiCRISPR v2 were obtained from Addgene (plasmid 38240 and plasmid 52961, respectively).

To establish stable cell lines expressing FRET biosensors by a transposon system, cells were cotransfected with pPB vector and pCMV-mPBase, which was obtained from the Wellcome Trust Sanger Institute, or with pT2A vector and pCAGGS-T2TP, which was a kind gift from Dr. Kawakami (National Institute for Genetics, Japan). One day after transfection,

the transfected cells were selected with 20 μg/ml of blasticidin S or 2 μg/ml puromycin, and then left for at least one week. For lentivirus-mediated introduction of the FRET biosensor gene, a cDNA encoding YPet, an YFP variant, was codon-diversified to prevent recombination between the YFP and CFP genes of the biosensor (Aoki, unpublished). For lentiviral production, HEK-293T cells were cotransfected with the pCSII-EF vector, psPAX2 from Addgene plasmid 12260, and pCMV-VSV-G-RSV-Rev, which was a kind gift from Dr. Miyoshi (RIKEN) by using Polyethyleneimine “Max” MW 40,000 (Polyscience Inc., Warrington, PA). As a retrovirus, pGP was used instead of psPAX2. Virus-containing media were collected at 48 hours after transfection, filtered, and used to infect target cells. Two days after infection, the infected cells were selected with 20 μg/ml blasticidin S. Cell lines expressing Eevee-S6K were additionally infected with retrovirus encoding mCherry-NLSx2 protein and selected with 1 mg/ml G418. Bulk of infected cells was used for imaging.

*Reagents.*

Gefitinib, SB-590885, AZD6244 and BI-D1870 were purchased from Symansis (Shanghai, China). PI-103 was purchased from Calbiochem (La Jolla, CA). Torin1 was purchased from Tocris Bioscience (Ellisville, MO). Rapamycin was purchased from LC Laboratories (Woburn, MA). PD0325901 was purchased from Wako (Osaka, Japan). Doxycyclin was obtained from LKT Laboratories (St. Paul, MN).

*Gene silencing using siRNAs.*

For the siRNA knockdowns, cells were transfected with 20 nM ON-TARGETplus siRNA pools (ThermoScientific) or 10 nM Silencer Select siRNAs (Life Technologies) using RNAiMAX Lipofectamine (Life Technologies) according to the manufacturer’s instructions. Cells were analysed 24 hours post-transfection.

*Raptor knockout using CRISPR/Cas9.*

For CRISPR/Cas9-mediated knockout of *RPTOR* gene, sgRNAs targeting *RPTOR* were designed using CRISPR Design Tools (http://crispr.mit.edu/). Targeting sequences are just after the start codon (#1) or region encoding $_{1191}$RVYDRR$_{1196}$ (#2 and #3) of *RPTOR*, which is required for the interaction with mTOR[35]. Oligo DNAs for the sgRNAs were annealed and inserted into lentiCRISPR v2 vector digested with *Bsm*BI restriction enzyme. sgRNA-Cas9 cassettes were introduced to HT-29 cells by lentivirus-mediated gene transfer. Infected cells were selected by 2 μg/ml Puromycin for at least two weeks and obtained bulk cell lines were analysed.

*Multiwell FRET imaging.*

FRET images were obtained and processed using essentially the same conditions and procedures as previously reported.[36] In brief, the bottoms of 96-well glass-based plates (Asahi Techno Glass, Tokyo, Japan) were coated with collagen type I (Nitta Gelatin Inc., Osaka, Japan) before plating cells. Cells expressing EKAREV-nls or Eevee-S6K/mCherry-NLSx2 were plated on the collagen-coated 96-well plate at a cell density of 3,000-4,000 cells/well. After cells attached to the glass base, the media was exchanged for 300 μl of imaging medium comprised of Medium 199 (Sigma-Aldrich) with 20 mM HEPES, 10% FBS and penicillin/streptomycin. Blasticidin S or/and puromycin were added to the imaging medium if necessary. Cells in the 96-well plates were cultured in CO2 incubators, and applied to a fluorescence microscope at the time point of image acquisition. All images were acquired with an inverted microscope (IX81; Olympus, Tokyo, Japan) equipped with a cooled CCD camera (Cool SNAP-K4; Roper Scientific), illumination systems (Spectra-X light engine; Lumencore, OR or CoolLED precisExcite; Molecular Devices, Sunnyvale, CA), an IX2-ZDC2 laser-based autofocusing system (Olympus), a MAC5000 controller for filter wheels and XY stage (Ludl Electronic Products, Hawthorne, NY), a chamlide WP stage incubator system (Live Cell Instrument, Seoul, Korea) and a GM-4000 CO2 supplier (Tokai-Hit, Fujinomiya, Japan). The following filters used for the dual emission imaging studies were obtained from Omega Optical (Brattleboro, VT): an XF1071 (440AF21) excitation filter, an XF2034 (455DRLP) dichroic mirror, and two emission filters (XF3075 (480AF30) for CFP

and XF3079 (535AF26) for YFP). Cells were imaged with an UPlanSApo x20 dry objective lens (Olympus). The same four positions were acquired in each well in the time course experiments. The microscope was controlled by Metamorph software (Universal Imaging, West Chester, PA).

*Image analysis.*

For background subtraction, all images were processed by the Flatten Background function included in the Metamorph software package. The background value was determined by Otsu's method and subtracted from the images.[37] After background subtraction, FRET/CFP ratio images were created to represent the FRET efficiency. Custom-made MATLAB program was used for subsequent image analyses as previously described[38]. Briefly, for the ERK FRET biosensor, EKAREV-nls, a fluorescence signal from the nucleus was used for the segmentation of each cell. For Eevee-S6K, red fluorescence from the nucleus in mCherry-NLSx2 was employed for the segmentation of each cell. The intensities of both the FRET and CFP channels from each single cell were measured to calculate the FRET/CFP ratio. Finally, the number of segmented areas was counted as the number of cells in each well. Metamorph software and MATLAB (version R2012a; Mathworks Inc., Natick, MA) were used for all these imaging procedures.

*Western blotting and antibodies.*

Cells were plated on collagen-coated 12-well plates, and one day after plating the cells were treated with inhibitors for 20 min or one day. Cells were then washed twice with cold PBS and lysed with lysis buffer containing 1% NP-40.[39] After centrifugation, the supernatants were analysed by SDS-polyacrylamide gel electrophoresis, followed by western blotting. The primary antibodies were as follows: p-ERK1/2(T202/Y204), ERK1/2, p-Akt(S473), pan-Akt, p-Rictor(T1135), TSC2, p-4E-BP1(T37/46), p-S6(S235/236) and S6 (Cell Signaling Technology, Beverly, MA). Raptor clone 1H6.2 was from MERCK/Millipore (Bedford, MA). Rictor (mAb, 1G11) was from Enzo Life Sciences (Farmingdale, NY). p-EGFR (Y1068) was from GenWay Biotech Inc. (Dan Diego, CA). EGFR from BD Biosciences (San Jose, CA).

The secondary antibodies were as follows: IRDye680LT- and IRDye800-conjugated anti-rabbit and anti-mouse IgG secondary antibodies, respectively (LI-COR Bioscience, Lincoln, NE). LI-COR blocking buffer (LI-COR Bioscience) was used to block the membranes and to dilute antibodies. Fluorescent signals were detected by an Odyssey Infrared Imager (LI-COR Bioscience).

*RNA isolation and qPCR.*

Cells were seeded onto collagen-coated 6-well culture plates at a density of 1 x $10^5$ cells/well and cultured overnight. The cells were treated with 0.1% DMSO or 0.1 μM PD0325901 for one day, and were washed with ice-cold PBS. Total RNAs were extracted using an RNeasy mini kit (Qiagen, Valencia, CA) according to the manufacturer's instructions. cDNA was prepared using a High Capacity cDNA Reverse Transcription Kit (Applied Biosystems, Foster City, CA) with random hexamer primers according to the manufacturer's instructions. The relative abundance of transcripts was measured by quantitative PCR using SYBR Green PCR mix (Applied Biosystems). The mRNA levels for each gene were normalized to that of GAPDH. The primers used were as follows. *hRheb*: forward 5' -ggaatcttctgctaaagaaaatcag-3', reverse 5' -gcatgaagacttgccttgtg-3'; *hTSC2*: forward 5' - cggatgcctacagcaggt-3', reverse 5' - agacgactcgctcgatgg-3'; *hDEPTOR*: forward 5' - tgagaggacagaggctatatgaaa-3', reverse 5' - tgaaggtgcgctcatacttg-3'; *hGAPDH*: forward 5' - gagtccactggcgtcttcac-3', reverse 5' - gttcacacccatgacgaaca-3'.

*RNA sequencing and sequence analysis.*

Total RNAs from cells treated with DMSO or PD0325901 were isolated by the method shown above. The library preparation and RNA sequencing were performed as previously described.[40] The CLC Genomics Workbench (www.clcbio.com) was used to map the reads, calculate the expression levels and determine the statistical significance of the results. Sequence reads of each data set were aligned to the human genome (Ensembl GRCh37.p13, Sep. 2013, version 75.37). The reads per kilobase (kb) of exon model per million mapped reads (RPKM) method was employed to calculate the gene expression.[41] Differentially

expressed genes (DEGs) were identified by the RNA-Seq Analysis function included in the CLC GWB platform. The False Discovery Rate (FDR) controlling approach was adopted to examine the significance of the differences in gene expression. The cut-off value for DEGs was FDR < 0.01.

*Numerical analysis.*

For non-linear regression, we utilized solver functions in Microsoft Excel or the lsqcurvefit function in MATLAB. Data visualization was performed by Excel or MATLAB. The R statistical computing environment was used for the cluster analysis. In Figures 1d, 1f, 2e, 2g, 3e and 3f, theoretical function described as shown below were used as a model function to fit the experimental data. The equation represents the relationship between the ERK or S6K activity and cell growth rate.

$$\text{growth rate} = min_g + amp_g \frac{IC50_g^{nH_g}}{\left(\frac{amp_A * IC50_A^{nH_A}}{Activity - min_A} - IC50_A^{nH_A}\right)^{\frac{nH_g}{nH_A}} + IC50_g^{nH_g}}$$

where *min* is the minimum, *amp* is the amplitude, *IC50* is the half maximum inhibitory concentration and *nH* is the Hill coefficient of the growth rate (g) or activity (A) of ERK or S6K. *Activity* is the FRET/CFP ratio of EKAREV-nls or Eevee-S6K. For data fitting, the difference between experimental value and theoretical value were calculated. Next residual sum of squares were minimized in order to obtain the best fitted curve. Because $min_A$, $min_g$ and $amp_A$ were determined unambiguously from experimental data, we fitted $amp_g$, $IC50_A$, $IC50_g$, $nH_A$, and $nH_g$ as parameters.

## Conflict of interest

The authors declare no conflict of interest.

## Acknowledgement

We are grateful to the members of the Matsuda Laboratory for their helpful input. We also thank K. Ui-Tei for the shRNA plasmids. Y. Inaoka, K. Hirano, A. Katsumata, N. Nishimoto,

N. Nonaka, and A. Kawagishi are also to be thanked for their technical assistance. KA and MM were supported by the Research Program of Innovative Cell Biology by Innovative Technology (the “Cell Innovation” Program) and Platform for Dynamic Approaches to Living System from the Ministry of Education, Culture, Sports, and Science, Japan. KA was supported by a Grant-in-Aid for Young Scientists (B) (23701052) and a Grant-in-Aid for Scientific Research (B). NK and YF were supported by a Grant-in-Aid for JSPS Fellows.

Supplementary Information accompanies this paper on the Oncogene website (http://www.nature.com/onc)

## References

1 Nishida E, Gotoh Y. The MAP kinase cascade is essential for diverse signal transduction pathways. *Trends Biochem Sci* 1993; **18**: 128–131.

2 Pylayeva-Gupta Y, Grabocka E, Bar-Sagi D. RAS oncogenes: weaving a tumorigenic web. *Nat Rev Cancer* 2011; **11**: 761–774.

3 Weinstein IB. Cancer. Addiction to oncogenes--the Achilles heal of cancer. *Science* 2002; **297**: 63–64.

4 Sharma SV, Settleman J. Oncogene addiction: setting the stage for molecularly targeted cancer therapy. *Genes Dev* 2007; **21**: 3214–3231.

5 Sharma SV, Bell DW, Settleman J, Haber DA. Epidermal growth factor receptor mutations in lung cancer. *Nat Rev Cancer* 2007; **7**: 169–181.

6 Neuzillet C, Tijeras-Raballand A, de Mestier L, Cros J, Faivre S, Raymond E. MEK in cancer and cancer therapy. *Pharmacol Ther* 2014; **141**: 160–171.

7 Solit DB, Garraway LA, Pratilas CA, Sawai A, Getz G, Basso A *et al*. BRAF mutation predicts sensitivity to MEK inhibition. *Nature* 2006; **439**: 358–362.

8 Singh A, Greninger P, Rhodes D, Koopman L, Violette S, Bardeesy N *et al*. A gene expression signature associated with "K-Ras addiction" reveals regulators of EMT and tumor cell survival. *Cancer Cell* 2009; **15**: 489–500.

9 Rebucci M, Michiels C. Molecular aspects of cancer cell resistance to chemotherapy. *Biochem Pharmacol* 2013; **85**: 1219–1226.

10 Sos ML, Fischer S, Ullrich R, Peifer M, Heuckmann JM, Koker M *et al*. Identifying genotype-dependent efficacy of single and combined PI3K- and MAPK-pathway inhibition in cancer. *Proc Natl Acad Sci U S A* 2009; **106**: 18351–18356.

11 Fritsche-Guenther R, Witzel F, Sieber A, Herr R, Schmidt N, Braun S *et al*. Strong negative feedback from Erk to Raf confers robustness to MAPK signalling. *Mol Syst Biol* 2011; **7**: 489.

12 Friday BB, Yu C, Dy GK, Smith PD, Wang L, Thibodeau SN *et al*. BRAF V600E disrupts AZD6244-induced abrogation of negative feedback pathways between extracellular signal-regulated kinase and Raf proteins. *Cancer Res* 2008; **68**: 6145–6153.

13 Hatzivassiliou G, Haling JR, Chen H, Song K, Price S, Heald R *et al*. Mechanism of MEK inhibition determines efficacy in mutant KRAS- versus BRAF-driven cancers. *Nature* 2013; **501**: 232–236.

14 Pratilas CA, Taylor BS, Ye Q, Viale A, Sander C, Solit DB *et al*. (V600E)BRAF is associated with disabled feedback inhibition of RAF-MEK signaling and elevated transcriptional output of the pathway. *Proc Natl Acad Sci U S A* 2009; **106**: 4519–4524.

15 Mirzoeva OK, Das D, Heiser LM, Bhattacharya S, Siwak D, Gendelman R *et al*. Basal subtype and MAPK/ERK kinase (MEK)-phosphoinositide 3-kinase feedback signaling determine susceptibility of breast cancer cells to MEK inhibition. *Cancer Res* 2009; **69**: 565–572.

16 Engelman JA, Chen L, Tan X, Crosby K, Guimaraes AR, Upadhyay R *et al*. Effective use of PI3K and MEK inhibitors to treat mutant Kras G12D and PIK3CA H1047R murine lung cancers. *Nat Med* 2008; **14**: 1351–1356.

17 Bean GR, Ganesan YT, Dong Y, Takeda S, Liu H, Chan PM *et al*. PUMA and BIM are required for oncogene inactivation-induced apoptosis. *Sci Signal* 2013; **6**: ra20.

18 LoRusso P, Shapiro G, Pandya SS, Kwak EL, Jones C, Belvin M *et al*. A first-in-human phase Ib study to evaluate the MEK inhibitor GDC-0973, combined with the pan-PI3K inhibitor GDC-0941, in patients with advanced solid tumors. *Journal of Clinical Oncology* 2012; **30**.

19 Speranza G, Kinders RJ, Khin S, Weil MK, Do KT, Horneffer Y *et al*. Pharmacodynamic biomarker-driven trial of MK-2206, an AKT inhibitor, with

AZD6244 (selumetinib), a MEK inhibitor, in patients with advanced colorectal carcinoma (CRC). *Journal of Clinical Oncology* 2012; **30**.

20 Komatsu N, Aoki K, Yamada M, Yukinaga H, Fujita Y, Kamioka Y *et al*. Development of an optimized backbone of FRET biosensors for kinases and GTPases. *Mol Biol Cell* 2011; **22**: 4647–4656.

21 LoRusso PM, Krishnamurthi SS, Rinehart JJ, Nabell LM, Malburg L, Chapman PB *et al*. Phase I pharmacokinetic and pharmacodynamic study of the oral MAPK/ERK kinase inhibitor PD–0325901 in patients with advanced cancers. *Clin Cancer Res* 2010; **16**: 1924–1937.

22 Thoreen CC, Kang SA, Chang JW, Liu Q, Zhang J, Gao Y *et al*. An ATP–competitive mammalian target of rapamycin inhibitor reveals rapamycin–resistant functions of mTORC1. *J Biol Chem* 2009; **284**: 8023–8032.

23 She QB, Halilovic E, Ye Q, Zhen W, Shirasawa S, Sasazuki T *et al*. 4E–BP1 is a key effector of the oncogenic activation of the AKT and ERK signaling pathways that integrates their function in tumors. *Cancer Cell* 2010; **18**: 39–51.

24 Roux PP, Ballif BA, Anjum R, Gygi SP, Blenis J. Tumor–promoting phorbol esters and activated Ras inactivate the tuberous sclerosis tumor suppressor complex via p90 ribosomal S6 kinase. *Proc Natl Acad Sci U S A* 2004; **101**: 13489–13494.

25 Carriere A, Romeo Y, Acosta–Jaquez HA, Moreau J, Bonneil E, Thibault P *et al*. ERK1/2 phosphorylate Raptor to promote Ras–dependent activation of mTOR complex 1 (mTORC1). *J Biol Chem* 2011; **286**: 567–577.

26 Rodriguez–Viciana P, Warne PH, Vanhaesebroeck B, Waterfield MD, Downward J. Activation of phosphoinositide 3–kinase by interaction with Ras and by point mutation. *EMBO J* 1996; **15**: 2442–2451.

27 Mendoza MC, Er EE, Blenis J. The Ras–ERK and PI3K–mTOR pathways: cross–talk and compensation. *Trends Biochem Sci* 2011; **36**: 320–328.

28 Klinger B, Sieber A, Fritsche–Guenther R, Witzel F, Berry L, Schumacher D *et al*. Network quantification of EGFR signaling unveils potential for targeted combination therapy. *Mol Syst Biol* 2013; **9**: 673.

29 Prahallad A, Sun C, Huang S, Di Nicolantonio F, Salazar R, Zecchin D *et al*. Unresponsiveness of colon cancer to BRAF(V600E) inhibition through feedback activation of EGFR. *Nature* 2012; **483**: 100–103.

30 Corcoran RB, Rothenberg SM, Hata AN, Faber AC, Piris A, Nazarian RM *et al.* TORC1 suppression predicts responsiveness to RAF and MEK inhibition in BRAF-mutant melanoma. *Sci Transl Med* 2013; **5**: 196ra198.

31 Yusa K, Rad R, Takeda J, Bradley A. Generation of transgene-free induced pluripotent mouse stem cells by the piggyBac transposon. *Nat Methods* 2009; **6**: 363-369.

32 Kawakami K, Noda T. Transposition of the Tol2 element, an Ac-like element from the Japanese medaka fish Oryzias latipes, in mouse embryonic stem cells. *Genetics* 2004; **166**: 895-899.

33 Miyoshi H, Blomer U, Takahashi M, Gage FH, Verma IM. Development of a self-inactivating lentivirus vector. *J Virol* 1998; **72**: 8150-8157.

34 Akagi T, Sasai K, Hanafusa H. Refractory nature of normal human diploid fibroblasts with respect to oncogene-mediated transformation. *Proc Natl Acad Sci U S A* 2003; **100**: 13567-13572.

35 Kim DH, Sarbassov DD, Ali SM, King JE, Latek RR, Erdjument-Bromage H *et al.* mTOR interacts with raptor to form a nutrient-sensitive complex that signals to the cell growth machinery. *Cell* 2002; **110**: 163-175.

36 Aoki K, Matsuda M. Visualization of small GTPase activity with fluorescence resonance energy transfer-based biosensors. *Nat Protoc* 2009; **4**: 1623-1631.

37 Otsu N. A threshold selection method from gray-level histograms. *IEEE Transactions on Systems, Man, and Cybernetics* 1979; **9**: 62-66.

38 Fujita Y, Komatsu N, Matsuda M, Aoki K. Fluorescence resonance energy transfer based quantitative analysis of feedforward and feedback loops in epidermal growth factor receptor signaling and the sensitivity to molecular targeting drugs. *FEBS J* 2014; **281**: 3177-3192.

39 Corcoran RB, Dias-Santagata D, Bergethon K, Iafrate AJ, Settleman J, Engelman JA. BRAF gene amplification can promote acquired resistance to MEK inhibitors in cancer cells harboring the BRAF V600E mutation. *Sci Signal* 2010; **3**: ra84.

40 Aoki K, Kumagai Y, Sakurai A, Komatsu N, Fujita Y, Shionyu C *et al.* Stochastic ERK activation induced by noise and cell-to-cell propagation regulates cell density-dependent proliferation. *Mol Cell* 2013; **52**: 529-540.

41 Mortazavi A, Williams BA, McCue K, Schaeffer L, Wold B. Mapping and quantifying mammalian transcriptomes by RNA-Seq. *Nat Methods* 2008; **5**: 621-628.

## Figure legends

**Figure 1**. Relation between ERK activity and cell growth rate. (a) FRET-based biosensor for ERK or S6K activity. (b) Experimental procedure for monitoring molecular activity and cell growth by multi-well plate time-lapse imaging. The montage image shows representative time courses of HT-29 cells treated with 0.1 μM AZD6244, a MEK1/2 inhibitor. (c and e) Dose dependencies of the cell growth rate (black) and ERK activity (magenta) on AZD6244 in HT-29 cells (c) and HCT116 cells (e). The growth rate and ERK activity on Day 1 are plotted with the s.d. (n = 3) and fitted curves. (d and f) Growth rates are plotted as a function of ERK activity in HT-29 cells (d) and HCT116 cells (f) with the s.d. (n = 3). Colors indicate the concentration of AZD6244. Dashed lines indicate the theoretical curves calculated by the fitted Hill-equation in panels c and e. See Materials and Methods for more details. (g) IC50 values of the cell growth rates in the indicated cell lines are plotted as a function of the IC50 values of ERK activity upon AZD6244 treatment with the s.d. (n = 3).

**Figure 2**. Involvement of the PI3K pathway on intrinsic resistance to MEKi in KRas-mutant cells. (a) Schematic view of the signaling pathway with inhibitors. (b) Procedure for calculating the relative resistance to inhibitors. The relative resistance to a particular inhibitor in a particular cell line was obtained by dividing the IC50 value in that cell line by the minimum IC50 value among all 8 cell lines. (c) The relative resistance to the 6 inhibitors among 8 cell lines was applied to complete linkage clustering analysis, and the resulting table is shown as a heat map. Black dashed lines indicate the borders of each cluster. White asterisks indicate the smallest relative resistance among the 8 cell lines against each inhibitor. The colors assigned to the different relative resistance values are shown on the right. (d and f) The effects of combinatorial treatment of MEKi and PI3Ki on the cell growth in HT-29 cells (d) and HCT116 cells (f) are shown as heat maps. The color hue on the bottom indicates the fold increase in cell number on day 3 relative to the number on day 0. The white dotted line on the heat map corresponds to the IC50 values of AZD6244 to ERK activity. (e and g) The cell growth rates are plotted as a function of ERK activity one day after treatment in HT-29 cells (e) and HCT116 cells (g) treated with MEKi and PI3Ki. Symbol shape and color represents concentration of AZD6244 and PI-103, respectively, as shown on the bottom.

Dashed lines indicate fitted curves by the the theoretical curve derived from Hill equation about growth rate and ERK activity.. For more details, see Materials and Methods.

**Figure 3**. Relation between S6K activity and cell growth rate. (a-d) Dose response of S6K activity in HT-29 cells (a and b) and HCT116 cells (c and d) upon treatment with AZD6244 (a and c) and PI-103 (b and d) for 3 days. Colored line represents time after drug treatment. Dotted horizontal line shows lower limit of S6K activity. (e and f) The cell growth rates are plotted as a function of S6K activity in HT-29 cells (e) and HCT116 cells (f) on Day 1. Symbol shape and color represents concentration of AZD6244 and PI-103 as shown on the right, respectively. Dashed lines indicate fitted curves. For more details, see Materials and Methods. (g) HT-29 cells (left) and HCT116 cells (right) were treated with serially diluted AZD6244 or 1 μM Torin1 for one day. Cell lysates were analyzed by immunoblotting for the levels of the indicated proteins. (h) pRictor/Rictor were plotted as a function of the AZD concentration with fitted curves in HT-29 cells (left) and HCT116 cells (right). pRictor/Rictor values at 1 μM Torin1 are also shown as a lower limit value.

**Figure 4**. Requirement of rapamycin-insensitive mTORC1 activity for cell growth. (a-f) The effects of PI-103 (a and d), Torin1 (b and e) and rapamycin (c and f) on the cell growth rate (black) and S6K activity (magenta) were measured in HT-29 cells (a-c) and HCT116 cells (d-f). The growth rate and S6K activity on Day 1 are plotted with the s.d. (n = 3). (g-i) Raptor depletion in A375 cells (g and j, left), A549 cells (h and j, middle) and HCT116 cells (i and j, right) by siRNA reduced the cell growth rates (g-i, left) and S6K activity measured by FRET imaging (g-i, right). Depletion of Raptor was confirmed by immunoblotting in A375 cells (j left), A549 cells ( j, middle) and HCT116 cells (j, right). ERK1/2 was utilized as a loading control. The numbers below the blots indicate the amounts of Raptor relative to negative control (NC) siRNA treatment. (k and l) Raptor knockout in HT-29 cells by CRISPR/Cas9 reduced the cell growth rates (k, left) and S6K activity measured by FRET imaging (k, right). Error bars represent the s.d. ($n \geq 6$). Depletion of Raptor was confirmed by immunoblotting (l). (m) The 4E-BP1 dominant negative mutant, 4E-BP1-4A, was induced by adding 1 μg/ml doxycycline (Dox.), and the cell numbers were analyzed to calculate the growth rate. Error bars represent the s.d. (n = 3).

**Figure 5**. Global changes in gene expression associated with the mTOR pathway. (a) Schemes for gene expression analysis. (b and c) M-A plot (the difference of average log intensities and the average of log intensities) of 0.1 μM PD0325901, a MEKi, in comparison to DMSO treatment in HT-29 cells (b) or HCT116 cells (c) (n = 2). Red and blue dots represent differentially up-regulated and down-regulated genes, respectively. (d) The expression levels of mTOR-related genes were altered by MEKi treatment. Differentially expressed genes that were identified in (b) or (c) were picked up and compared between HT-29 cells (blue) and HCT116 cells (red). (e) The cells indicated on the right were treated with 0.1 μM PD0325901 or DMSO for one day. These mRNA levels were subjected to qPCR analysis. The mean gene expression levels are shown with the s.d. (n = 3). Significant differences between BRaf-mutant cells and KRas-mutant cells ($p < 1x10^{-5}$, ANOVA) are indicated with a single asterisk. N.S. indicates no significance.

**Figure 6**. Model explaining the differential sensitivity to MEKi between oncogenic BRaf-mutant cancer cells (a) and KRas-mutant cancer cells (b). In this model, ERK upregulates mTORC1 via transcriptional regulation of the gene expressions related to mTORC1 signalling. Cell growth is mainly determined by mTORC1 activity.

## Supplementary figure legends

**Figure S1**. Reactivation of ERK in HCT116 cells treated with a MEK inhibitor. ERK activities before (blue dots) and after AZD6244 treatment (20 min, cyan dots; one day, green dots) are plotted as a function of the AZD6244 concentration with the s.d. (n = 3). Lines demonstrate fitted curves with the Hill-equation. Note that the IC50 values on Day 1 are higher than that at 20 min after MEKi treatment, indicating reactivation of ERK activity.

**Figure S2**. ERK activity distribution under combinatorial inhibition of MEK and PI3K. HT-29 cells (a) and HCT116 cells (b) were treated with combination of AZD6244 and PI-103 for 1 day. Distributions of the ERK activity from each single cell were shown as histograms.

Colored lines represent concentration of AZD6244 as shown on the below box. Concentrations of PI-103 were shown on the top of the each plot.

**Figure S3**. Effects of combinatorial MEK and PI3K inhibition on S6K activity and cell growth. (a-d) HT-29 cells (a and b) and HCT116 cells (c and d) were treated with AZD6244 and PI-103. The S6K activity (a and c) and growth rate on Day 1 (b and d) are represented as heatmaps. White dotted lines and black dotted lines indicate the IC50 value of AZD6244 for ERK activity and the IC50 value of PI-103 for S6K activity in each cell line.

**Figure S4**. S6K activity distribution under combinatorial inhibition of MEK and PI3K. HT-29 cells (a) and HCT116 cells (b) were treated with combination of AZD6244 and PI-103 for 1 day. Distributions of the S6K activity from each single cell were shown as histograms. Colored lines represent concentration of AZD6244 as shown on the below box. Concentrations of PI-103 were shown on the upper of the each plot. Of note, untreated HCT116 cells showed broader and biased S6K activity distribution compared to untreated HT-29 cells.

**Figure S5**. Rictor phosphorylation upon MEK inhibitor treatment. (a and b) Colo205 cells (a) and LIM1215 cells (b) were treated with 0.1% DMSO, 1 μM AZD6244, 1 μM PI-103, 1 μM Torin1, or 250 nM rapamycin for 20 min or one day. The cell lysates were subjected to immunoblotting with the antibodies indicated at left. (c and d) Quantification of Rictor phosphorylation in Colo205 (c) and LIM1215 (d). Colo205 cells, which were sensitive to MEKi, showed a clear reduction of the pRictor level upon MEKi treatment as well as that obtained in Torin1 treatment, whereas LIM1215 cells, which showed strong resistance to MEKi, did not.

**Figure S6**. Effect of DEPTOR depletion on S6K activity and cell growth. (a-d) HT-29 cells expressing S6K FRET biosensor were treated with scrambled siRNA (a and b) or siDEPTOR (c and d) for one day, followed by MEKi treatment. S6K activity (a and c) and cell growth rate (b and d) are plotted as a function of AZD6244 concentration, showing that DEPTOR is dispensable for MEKi-induced S6K suppression and cell growth arrest. (e) Expression levels of DEPTOR in control or siDEPTOR-treated HT-29 cells were quantified by qPCR.

**Figure S7**. Effect of TSC2 depletion on S6K activity and cell growth. (a-d) A375 cells expressing the S6K FRET biosensor were treated with scrambled siRNA (a and b) or siTSC2 (c and d) for one day, followed by MEKi treatment. The S6K activity (a and c) and cell growth rate (b and d) are plotted as a function of AZD6244 concentration, showing that TSC2 is dispensable for MEKi-induced S6K suppression and cell growth arrest. (e) Immunoblotting analysis confirmed the TSC2 expression in control or siTSC2-treated A375 cells. The numbers on the bottom are the values of TSC2 expression relative to scrambled siRNA treatment.

**Figure S8**. Effects of MEK inhibitor treatment on Akt phosphorylation. HT-29 cells and HCT116 cells cultured in the presence of 10% serum were treated with the indicted concentration of AZD6244 or 1 μM Torin1 for 1 day. The cell lysates were subjected to immunoblotting with the antibodies indicated on the left. MEK inhibitor treatment did not increase pAkt level in both HT-29 and HCT116 cells.

**Figure S9**. Effects of combinatorial inhibiton of MEK and EGFR on S6K activity and cell growth. (a-d) HT-29 cells (a and b) and HCT116 cells (c and d) were treated with AZD6244 and Gefitinib. The S6K activity (a and c) and growth rate on Day 1 (b and d) are represented as heatmaps. White dotted lines indicate the IC50 value of AZD6244 for ERK activity in each cell line.

**Figure S10**. Inhibition of EGF-induced phosphorylation of EGFR, Akt and ERK by Gefitinib. Serum-starved HT-29 cells and HCT116 cells were treated with 10 ng/ml EGF and 1 μM PD153035, an EGFR inhibitor, 10 μM or 1 μM Gefitinib for 5 minutes. The cell lysates were subjected to immunoblotting with the antibodies indicated on the left.

**Table S1**. Mutation statuses of *KRas, BRaf, PIK3CA* and *PTEN* in cell lines used in this study.

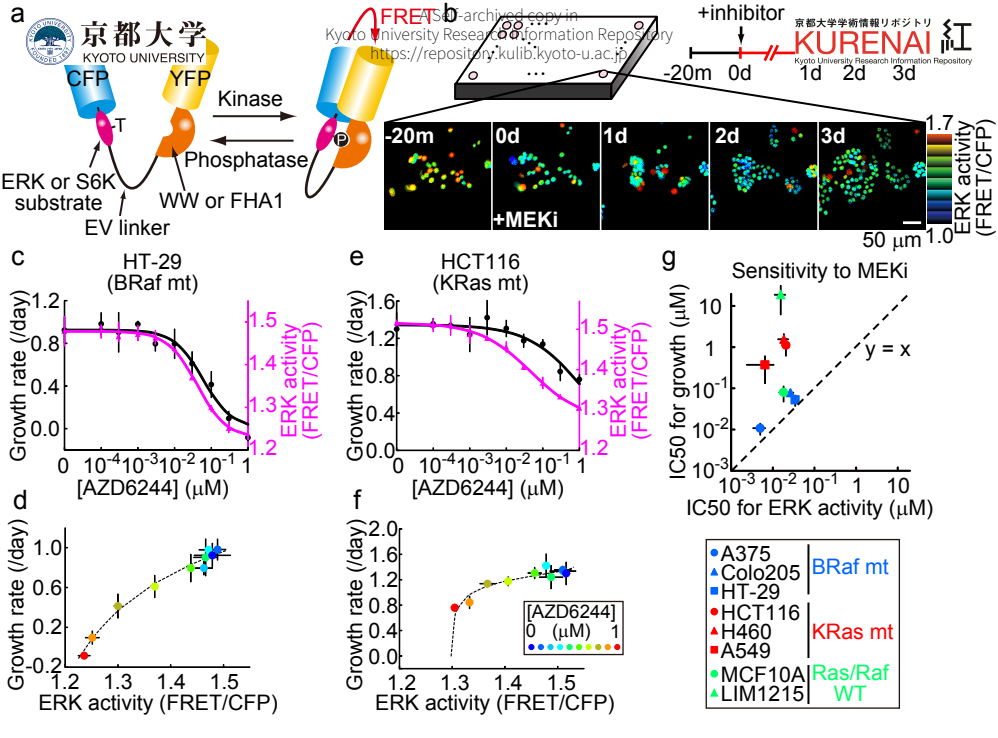


Fig.1

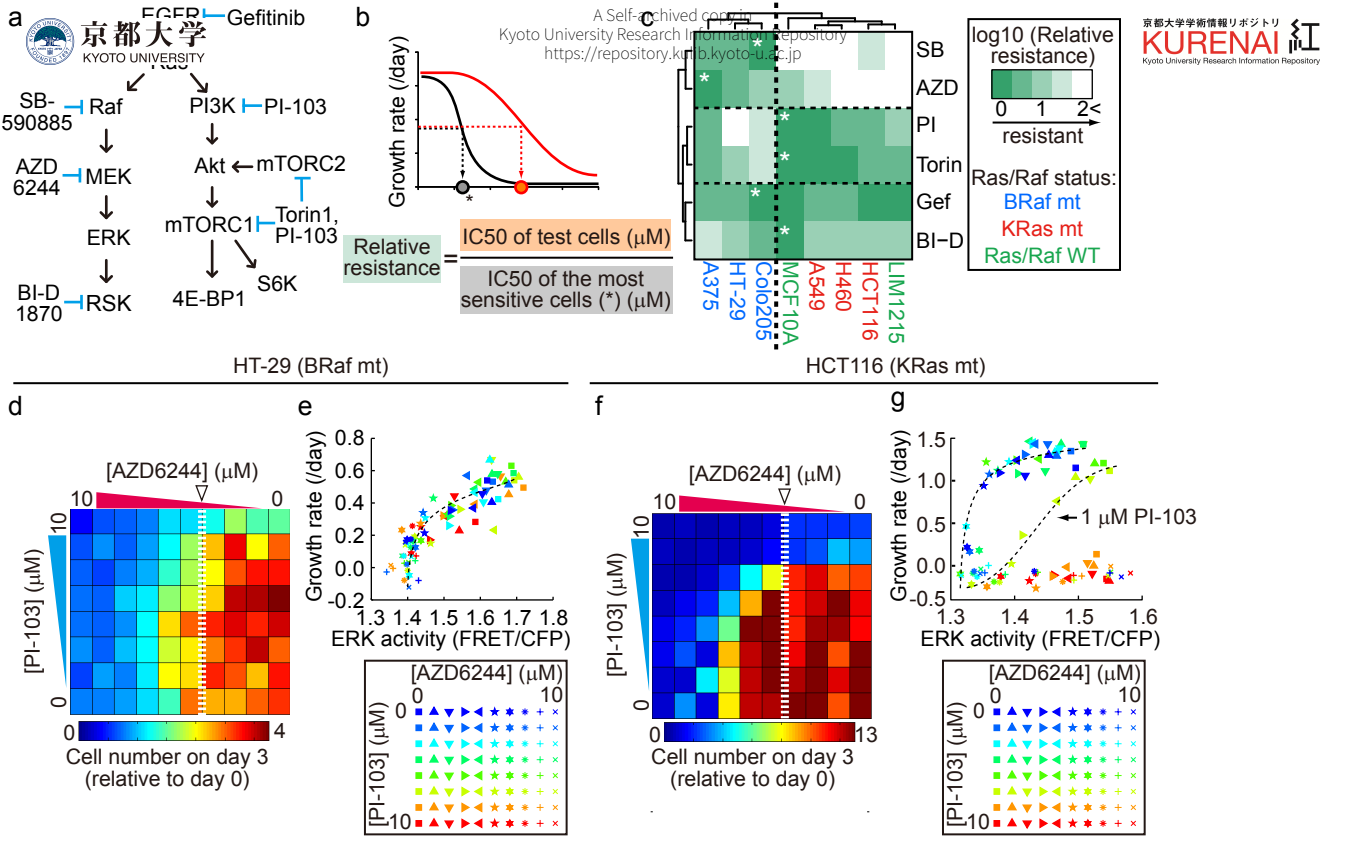


Fig.2

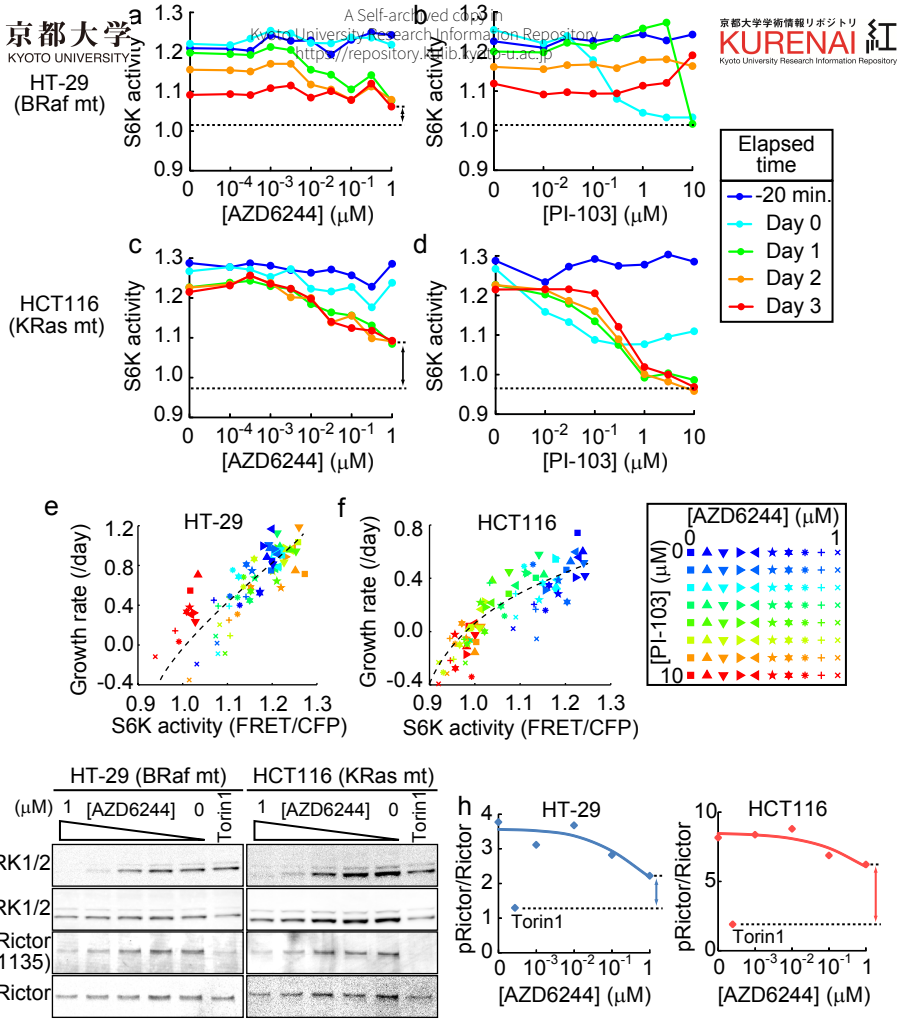





Fig.3

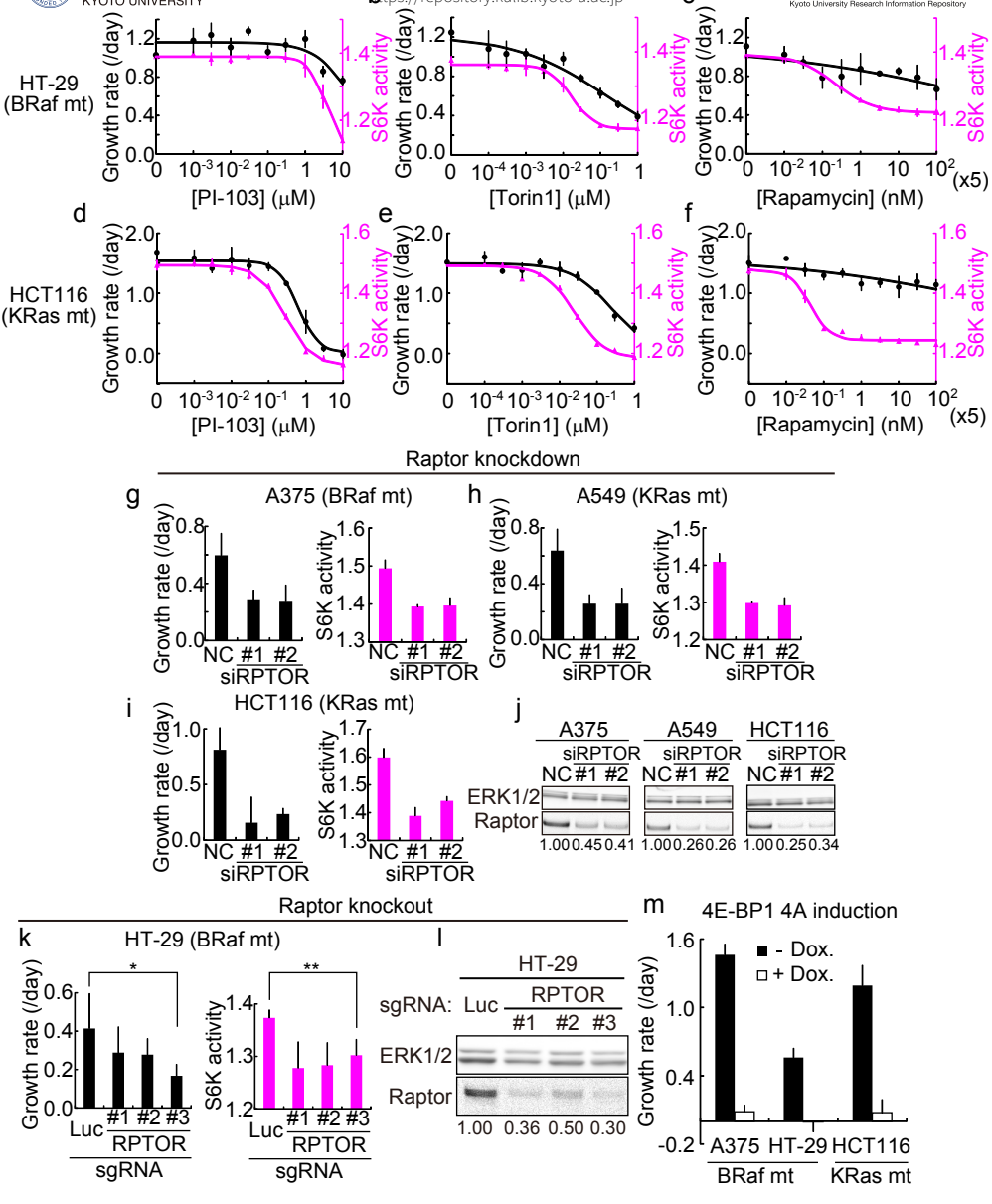

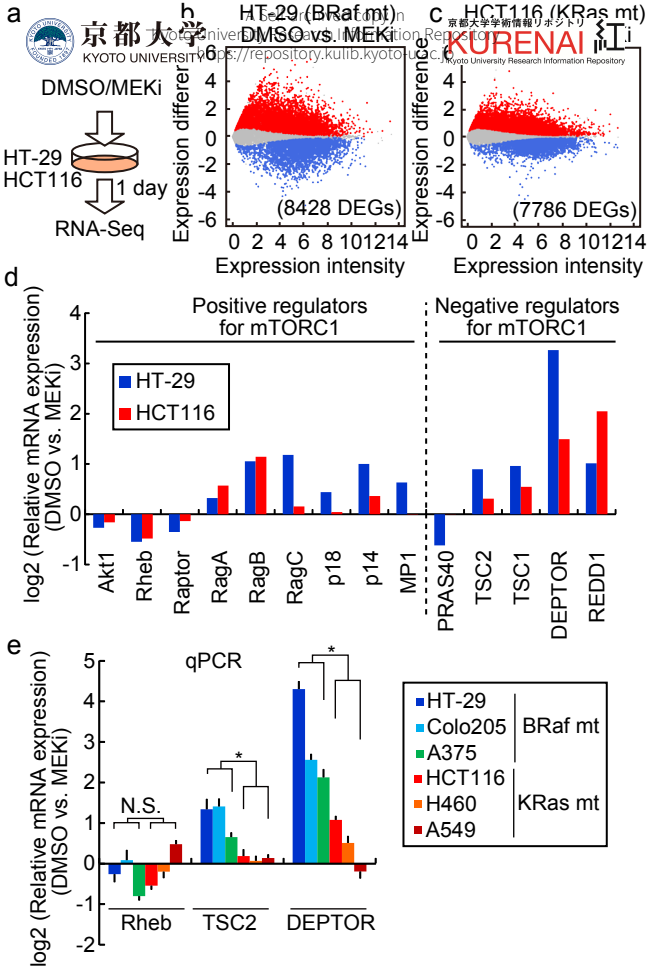


Fig.5

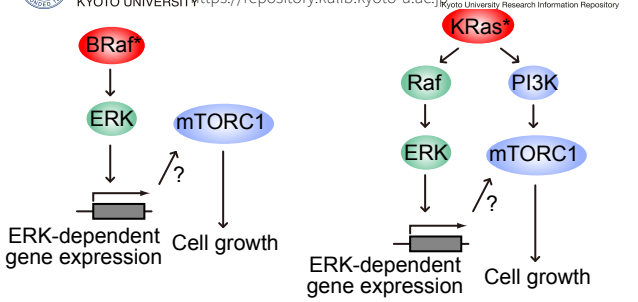


Fig.6

**Supplementary Information**

# mTORC1 upregulation via ERK-dependent gene expression change confers intrinsic resistance to MEK inhibitors in oncogenic KRas-mutant cancer cells.

Naoki Komatsu[1], Yoshihisa Fujita[2], Michiyuki Matsuda[1,2], and Kazuhiro Aoki[3]

**Supplementary Figure S1:** Reactivation of ERK in HCT116 cells treated with a MEK inhibitor.

**Supplementary Figure S2**: ERK activity distribution under combinatorial inhibition of MEK and PI3K.

**Supplementary Figure S3**: Effects of combinatorial MEK and PI3K inhibition on S6K activity and cell growth.

**Supplementary Figure S4**: S6K activity distribution under combinatorial inhibition of MEK and PI3K.

**Supplementary Figure S5**: Rictor phosphorylation upon MEK inhibitor treatment.

**Supplementary Figure S6**: Effect of DEPTOR depletion on S6K activity and cell growth.

**Supplementary Figure S7**: Effect of TSC2 depletion on S6K activity and cell growth.

**Supplementary Figure S8**: Effects of MEK inhibitor treatment on Akt phosphorylation.

**Supplementary Figure S9**: Effects of combinatorial inhibiton of MEK and EGFR on S6K activity and cell growth.

**Supplementary Figure S10**: Inhibition of EGF-induced phosphorylation of EGFR, Akt and ERK by Gefitinib.

**Supplementary Table 1**: Mutation statuses of *KRas*, *BRaf*, *PIK3CA* and *PTEN* in cell lines used in this study.

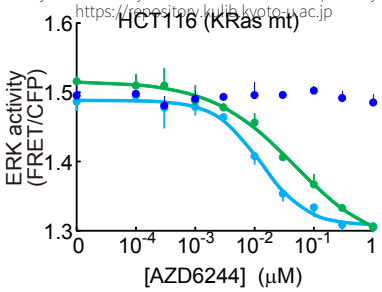


**Supplementary Figure S1. Reactivation of ERK in HCT116 cells treated with a MEK inhibitor.** ERK activities before (blue dots) and after AZD6244 treatment (20 min, cyan dots; one day, green dots) are plotted as a function of the AZD6244 concentration with the s.d. (n = 3). Lines demonstrate fitted curves with the Hill-equation. Note that the IC50 values on Day 1 are higher than that at 20 min after MEKi treatment, indicating reactivation of ERK activity.

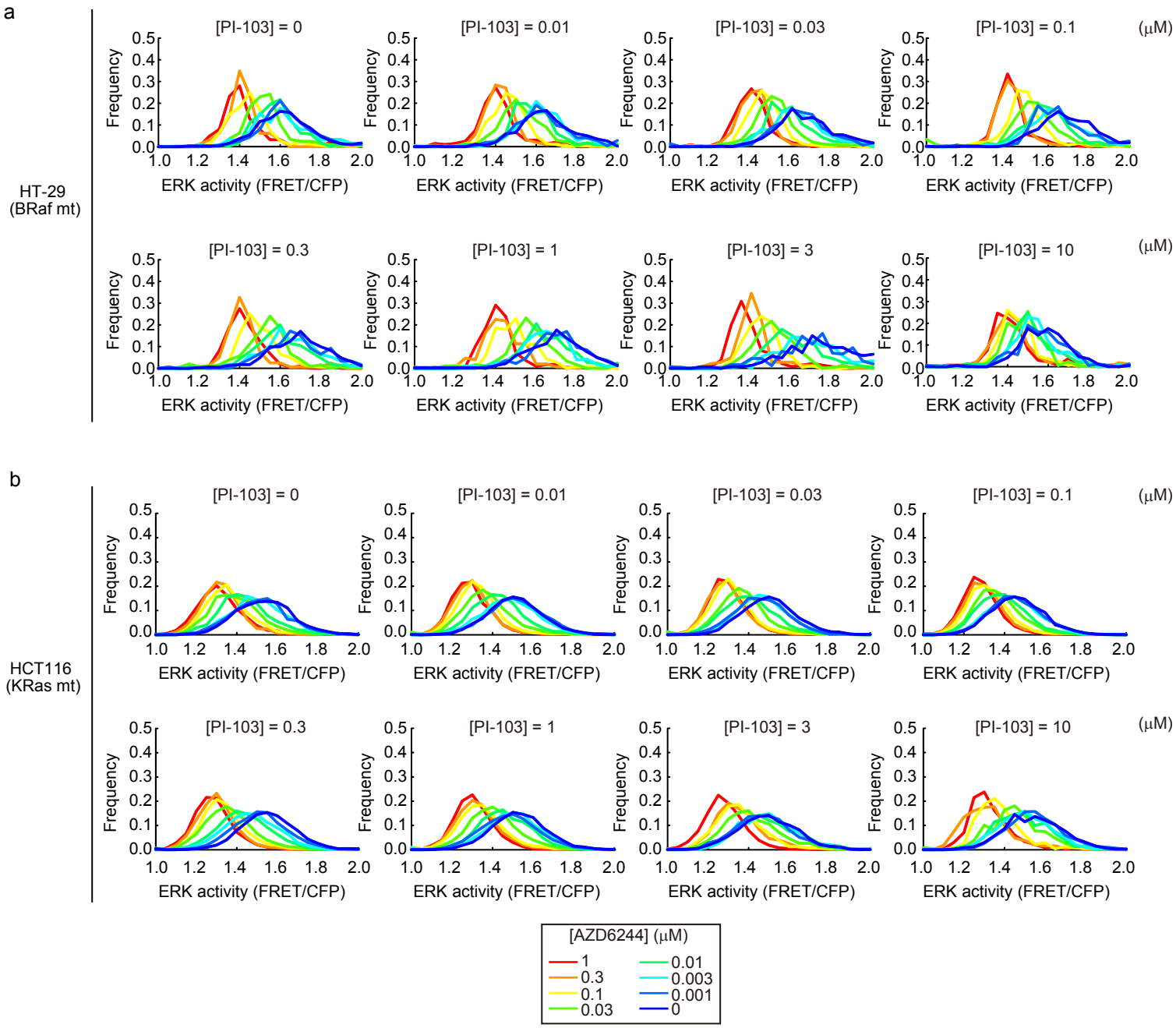


**Supplementary Figure S2. ERK activity distribution under combinatorial inhibition of MEK and PI3K.**

HT-29 cells (a) and HCT116 cells (b) were treated with combination of AZD6244 and PI-103 for 1day. Distributions of the ERK activity from each single cell were shown as histograms. Colored lines represent concentration of AZD6244 as shown on the below box. Concentrations of PI-103 were shown on the upper of the each plot.

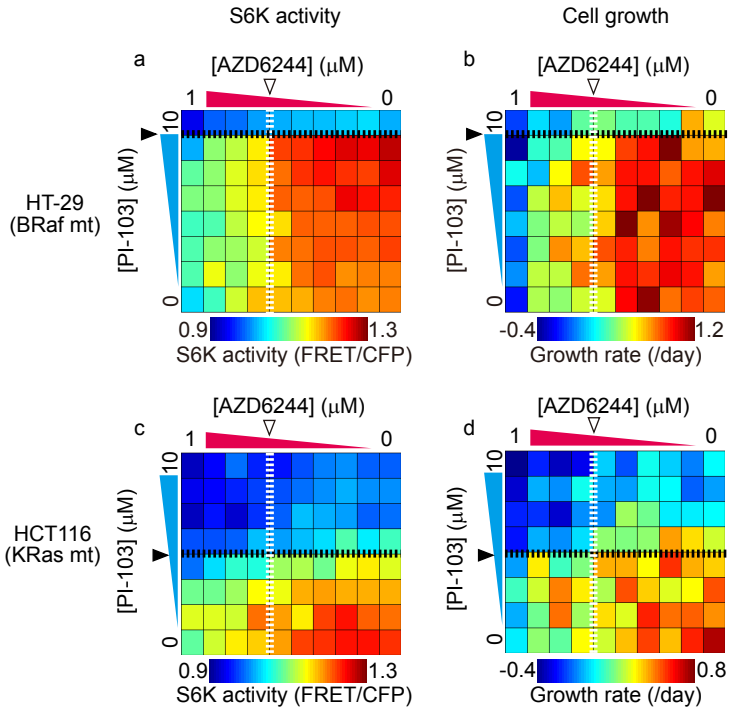


**Supplementary Figure S3. Effects of combinatorial MEK and PI3K inhibition on S6K activity and cell growth.**
(a-d) HT-29 cells (a and b) and HCT116 cells (c and d) were treated with AZD6244 and PI-103. The S6K activity (a and c) and growth rate on Day 1 (b and d) are represented as heatmaps. White dotted lines and black dotted lines indicate the IC50 value of AZD6244 for ERK activity and the IC50 value of PI-103 for S6K activity in each cell line.

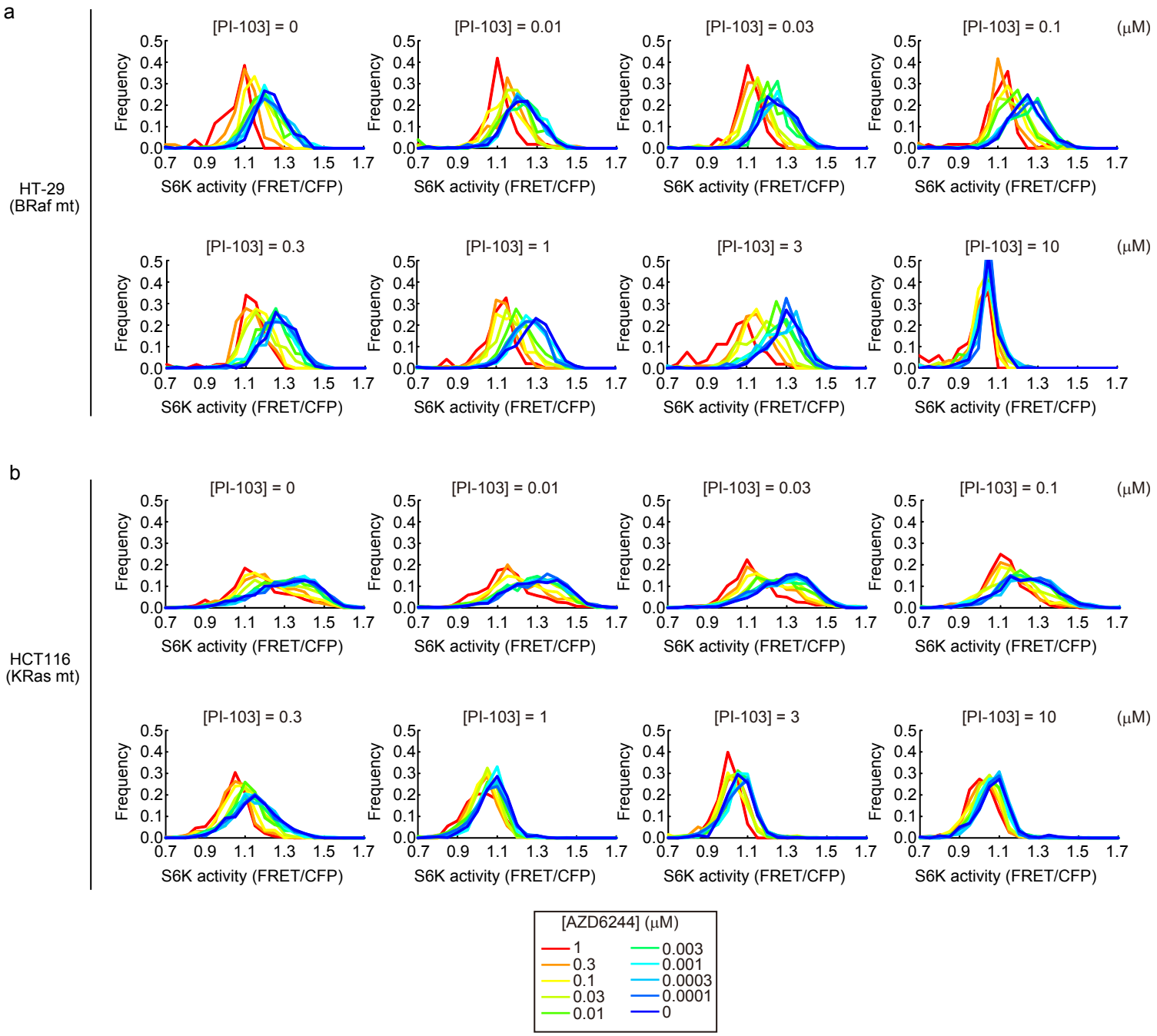


**Supplementary Figure S4. S6K activity distribution under combinatorial inhibition of MEK and PI3K. HT-29 cells** (a) and HCT116 cells (b) were treated with combination of AZD6244 and PI-103 for 1day. Distributions of the S6K activity from each single cell were shown as histograms. Colored lines represent concentration of AZD6244 as shown on the below box. Concentrations of PI-103 were shown on the upper of the each plot. Of note, untreated HCT116 cells showed broader and biased S6K activity distribution compared to untreated HT-29 cells.

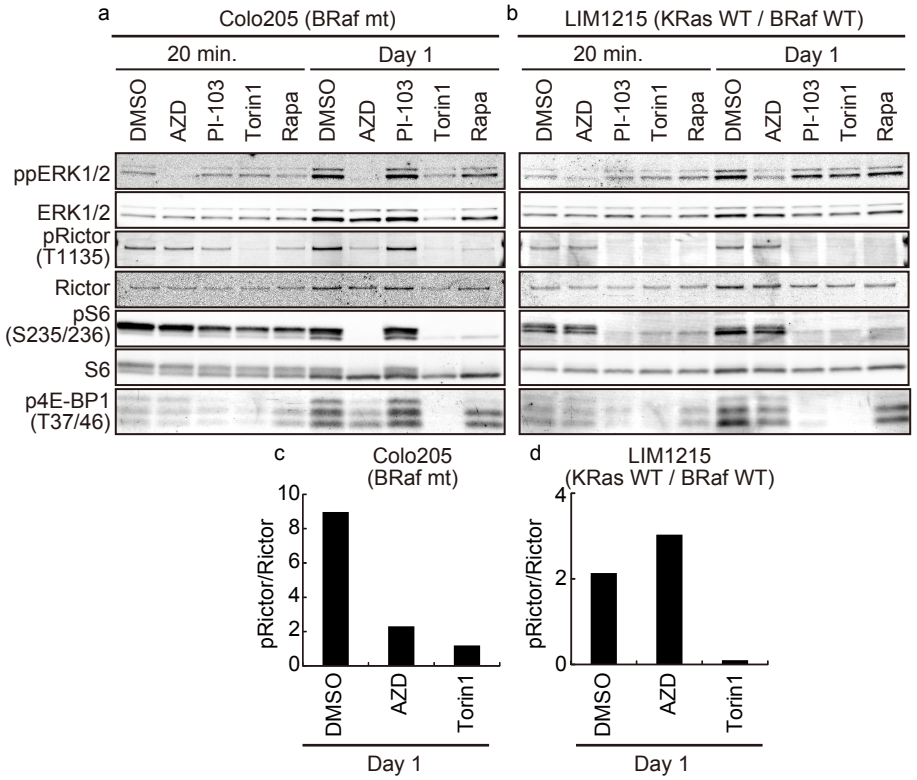


**Supplementary Figure S5. Rictor phosphorylation upon MEK inhibitor treatment.** (a and b) Colo205 cells (a) and LIM1215 cells (b) were treated with 0.1% DMSO, 1 μM AZD6244, 1 μM PI-103, 1 μM Torin1, or 250 nM Rapamycin for 20 min or one day. The cell lysates were subjected to immunoblotting with the antibodies indicated at left. (c and d) Quantification of Rictor phosphorylation in Colo205 (c) and LIM1215 (d). Colo205 cells, which were sensitive to MEKi, showed a clear reduction of the pRictor level upon MEKi treatment as well as that obtained in Torin1 treatment, whereas LIM1215 cells, which showed strong resistance to MEKi, did not.

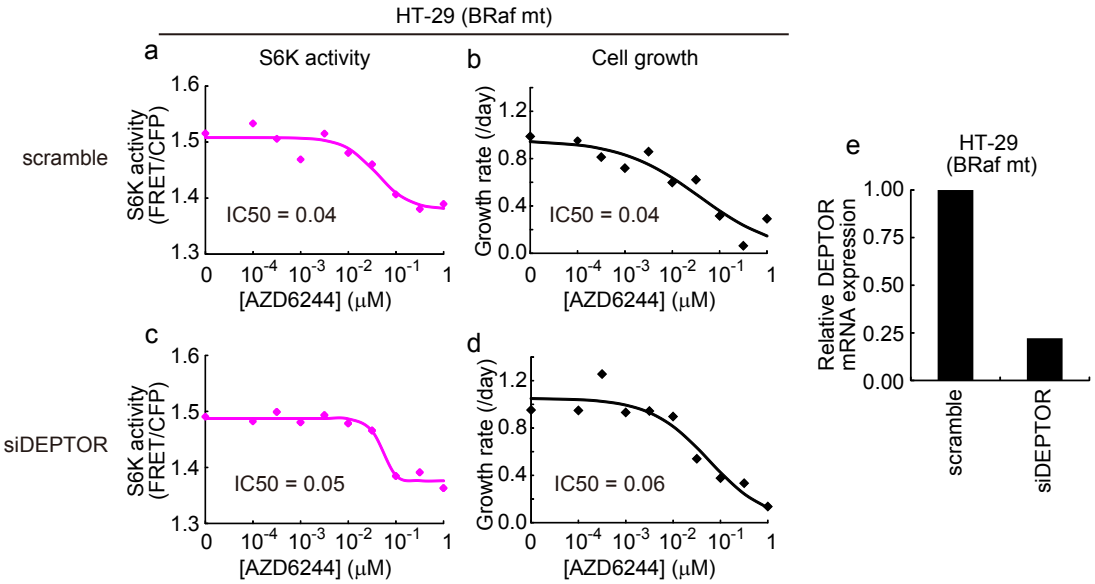


**Supplementary Figure S6. Effect of DEPTOR depletion on S6K activity and cell growth.** (a-d) HT-29 cells expressing S6K FRET biosensor were treated with scrambled siRNA (a and b) or siDEPTOR (c and d) for one day, followed by MEKi treatment. S6K activity (a and c) and cell growth rate (b and d) are plotted as a function of AZD6244 concentration, showing that DEPTOR is dispensable for MEKi-induced S6K suppression and cell growth arrest. (e) Expression levels of DEPTOR in control or siDEPTOR-treated HT-29 cells were quantified by qPCR.

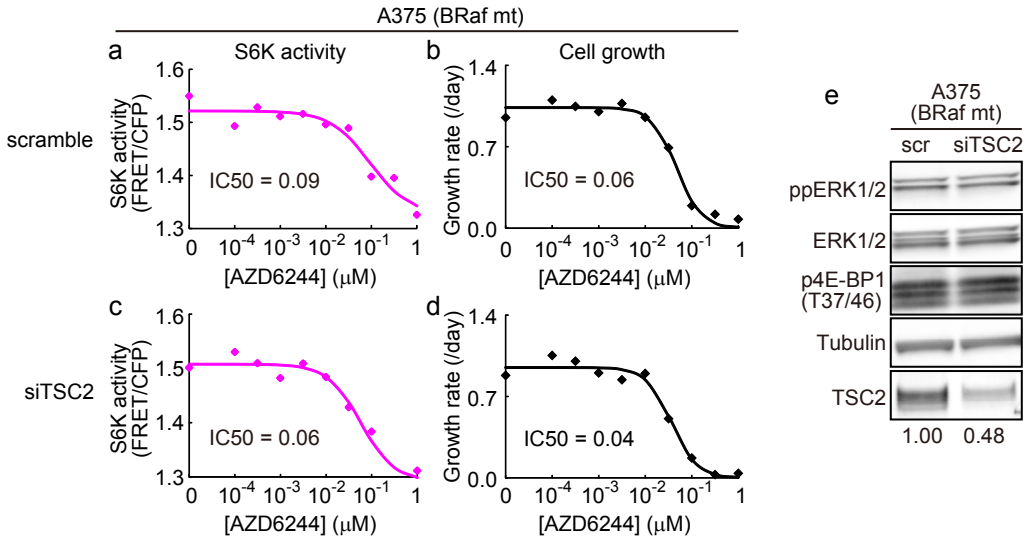


**Supplementary Figure S7. Effect of TSC2 depletion on S6K activity and cell growth.** (a-d) A375 cells expressing the S6K FRET biosensor were treated with scrambled siRNA (a and b) or siTSC2 (c and d) for one day, followed by MEKi treatment. The S6K activity (a and c) and cell growth rate (b and d) are plotted as a function of AZD6244 concentration, showing that TSC2 is dispensable for MEKi-induced S6K suppression and cell growth arrest. (e) Immunoblotting analysis confirmed the TSC2 expression in control or siTSC2-treated A375 cells. The numbers on the bottom are the values of TSC2 expression relative to scrambled siRNA treatment.

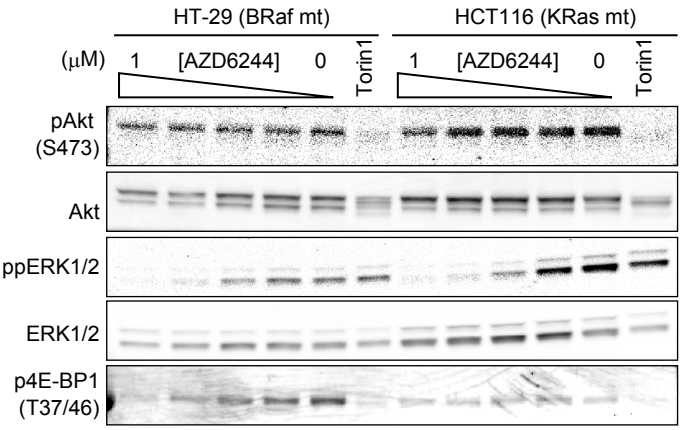


**Supplementary Figure S8. Effects of MEK inhibitor treatment on Akt phosphorylation.**

HT-29 cells and HCT116 cells cultured in the presence of 10% serum were treated with the indicted concentration of AZD6244 or 1 μM Torin1 for 1 day. The cell lysates were subjected to immunoblotting with the antibodies indicated on the left. MEK inhibitor treatment did not increase pAkt level in both HT-29 and HCT116 cells.

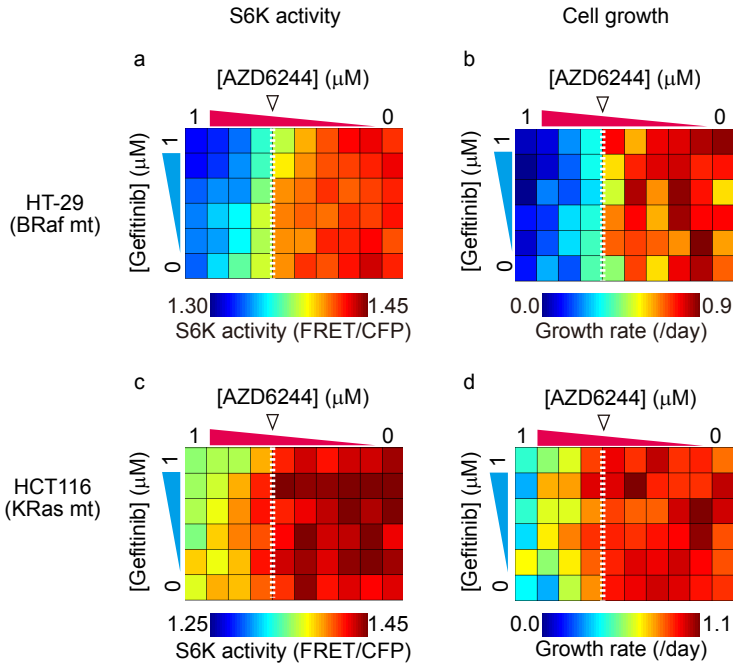


**Supplementary Figure S9. Effects of combinatorial inhibiton of MEK and EGFR on S6K activity and cell growth.**
(a-d) HT-29 cells (a and b) and HCT116 cells (c and d) were treated with AZD6244 and Gefitinib. The S6K activity (a and c) and growth rate on Day 1 (b and d) are represented as heatmaps. White dotted lines indicate the IC50 value of AZD6244 for ERK activity in each cell line.

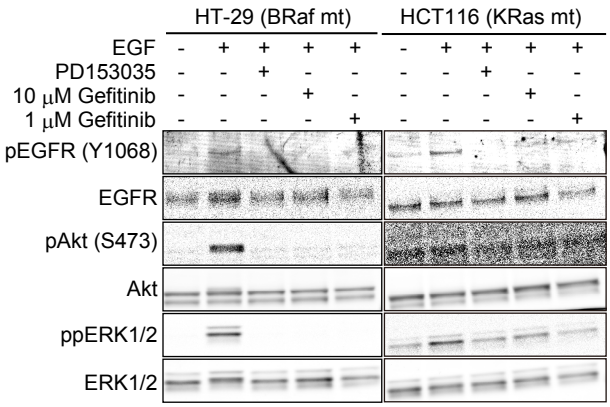


**Supplementary Figure S10. Inhibition of EGF-induced phosphorylation of EGFR, Akt and ERK by Gefitinib.**

Serum-starved HT-29 cells and HCT116 cells were treated with 10 ng/ml EGF and 1 μM PD153035, an EGFR inhibitor, 10 μM or 1 μM Gefitinib for 5 minutes. The cell lysates were subjected to immunoblotting with the antibodies indicated on the left.

**Supplementary Table 1. Mutation statuses of *KRas*, *BRaf*, *PIK3CA* and *PTEN* in cell lines used in this study.**

| Cell line * | Origin | KRas | BRaf | PIK3CA | PTEN |
|---|---|---|---|---|---|
| NCI-H460 | Lung | Q61H | WT | E545K | WT |
| A549 | Lung | G12S | WT | WT | WT |
| HCT116 | Colon | G13D | WT | H1047R | WT |
| HT-29 | Colon | WT | V600E | P449T | WT |
| Colo205 | Colon | WT | V600E | WT | WT |
| A375 | Skin | WT | V600E | WT | WT |
| LIM1215 † | Colon | WT | WT | WT | WT |
| MCF10A ‡ | Breast | WT | WT | WT | WT |

* Mutations are referenced from COSMIC database, http://cancer.sanger.ac.uk/cancergenome/projects/cosmic/
† Jhawer M et al., 2008
‡ Kadota M et al., 2010